JOURNAL OF GEOPHYSICAL RESEARCH, VOL. 101, NO. D8, PAGES 12,819–12,826, MAY 27, 1996

On the determination of scale ranges for precipitation fields

Frédéric Fabry

Advanced Study Program, National Center for Atmospheric Research, Boulder, Colorado

Abstract. To test some recent theories on the nature of precipitation structure, data were collected using radar and a newly developed "sonic" gauge to investigate precipitation variability at small scales. Results show that the structure of precipitation below a few tens of meters has very different statistics than at larger scales. Interpretation of vertically pointing radar data suggests that, at small scales, a mixing-like process occurs because of the differential fall speed of hydrometeors, which results in the destruction of small-scale structure. It is also shown that convection in the melting layer seems to recreate some of the structure that had been lost as snow fell. Finally, over scales of meteorological interest, at least four distinct regimes in precipitation variability can be identified.

Introduction

In recent years, new approaches based on self-similarity or scaling have been used to study the spatial and temporal variability of precipitation [*Schertzer and Lovejoy*, 1987; *Gupta and Waymire*, 1993 and references therein]. Contrary to previous models of rainfall variability based on a cellular approach (convective cells inside mesoscale precipitation areas inside synoptic areas [*Austin and Houze*, 1972]), scaling theories try to explain the variability at all scales as one continuous cascade-like process. There is considerable evidence that, over a large range of scales, these theories are successful in describing precipitation variability [*Tessier et al.*, 1993; *Over and Gupta*, 1994].

The proposed reasons for the success of this approach and the origin of the scaling properties observed in rain are as follows. It has been argued by *Lovejoy and Schertzer* [1986] that scaling in wind velocity over a considerable range of scales naturally arises from the Navier-Stokes equation. Since precipitation is so much coupled with wind, first in its formation and growth in updraft regions and then as hydrometeors are carried along by the turbulent wind, it seems natural to assume that precipitation statistics will mimic the statistical properties of wind, perhaps including its scaling. Furthermore, *Tessier et al.* [1993] also argued that any fundamental break in the scaling symmetry in wind will be reflected in precipitation and that the scaling range observed in the former should also be present in the latter. Since wind has been showed to be scaling down to dissipation scales (a few millimeters), so should the precipitation field.

Such a result, if verified, could be important for more accurately modeling the precipitation field. It also has some intriguing practical consequences, for example, in the measurement of precipitation by radar. Radar returns from precipitation are highly fluctuating because of the constructive and destructive interference of individual scatterers. The basis behind the measurement of the reflectivity Z from a region is that if the scatterers are randomly distributed in the illuminated volume, then the reflectivity can be derived directly by averaging these fluctuations [*Marshall and Hitschfeld*, 1953]. However, scaling implies a high degree of organization and clustering in the precipitation field down to sub-wavelength scales, which is in contradiction with the supposition of uniform randomness. As a result, the approximation used for the past 40 years to measure Z may be subject to limitations on its validity, and new approaches may have to be used [*Duncan et al.*, 1993].

The link between wind and precipitation, particularly at small scales, is not a perfect one. For example, hydrometeors have inertia and fall speeds and hence cannot be considered perfect passive tracers being advected by the wind. As a result, scaling in the precipitation field might stop at much larger scales than expected. Several researchers have also challenged the applicability of scaling theories at all scales [e.g., *Kumar and Foufoula-Georgiou*, 1993]. Still, measurements of precipitation variability at very small time scales or spatial scales are scarce [*Lovejoy and Schertzer*, 1990; *Georgakakos et al.*, 1994], and more are needed in order to verify if a scaling break in the precipitation field can be observed. This paper reports on attempts to observe and study the variability of precipitation at small scales.

Achieving the Best Space-Time Resolution

Most current meteorological instruments are inappropriate to study the small-scale variability (distances of the order of a meter and times shorter than a second) of the precipitation field. Large footprint instruments, like radar, smear the variability of the precipitation field over at least several tens of meters. Small footprint instruments, like precipitation gauges, are too quantized and require significant integration time to obtain a statistically significant measurement. During this averaging time, precipitation is advected, and the need for smoothing in time results in a reduced spatial resolution. Furthermore, an additional constraint arises when the precipitation field must be modeled by multifractal approaches [e.g., *Tessier et al.*, 1993; *Gupta and Waymire*, 1993]. In multifractal modeling, precipitation rate is assumed to be a field, like pressure. At very small scales, the field approximation of precipitation breaks down as this "continuous" flux of water becomes individual hydrometeors. Imagine a needlepoint-size sensor sampling a 1-mm hr^{-1} rainfall. Such a sensor will detect short bursts (less than a millisecond) of rain falling at a few meters per second or tens of millions of millimeters per hour (when raindrops hit the sensor) followed by long periods exceeding tens of minutes with no precipitation at all. Clearly, in this case, the continuous field approximation of rainfall is not valid. A field approximation

Paper number 96JD00718.
0148-0227/96/96JD-00718$09.00

Table 1. Number of Drops and of Significant Drops Falling Over a Given Precipitation Sensor Area per Natural Averaging Time for a 1 mm hr^{-1} Rainfall Assuming a Marshall-Palmer Drop Size Distribution.

Sensor Area	Number of Drops	Number of Drops >0.5 mm*	Natural Averaging Time, s
10 m^2	5620	2390	0.32
1 m^2	78	76	0.1
0.25 m^2	22	9.5	0.05
0.1 m^2	5.6	2.4	0.032
0.032 m^2 (gauge)	1.0	0.4	0.018

*The significant drops (drops of diameter >0.5 mm) contribute to 94% of the rain flux.

of precipitation is only valid over spaces and times where the contribution of several tens of hydrometeors can be averaged. Therefore, to resolve small-scale variability, the ideal sensor size must be within these two extremes to obtain measurements with the best "real" space (or time) resolution.

Horizontal movement of precipitation patterns provides a natural timescale to space scale conversion. Radar echoes of precipitation shafts generally move at a similar velocity independently of the height at which they are observed [*Marshall*, 1953]. A typical speed of echo movement is about 10 m s^{-1}. As a result, measurements 1 s long smooth the spatial structure of precipitation over scales of the order of 10 m. (Scale independent fixed velocities are used for time to space conversions throughout this paper; the appendix presents the reasons behind this choice) This suggests that for optimum sensor design, there is a natural averaging time period for a given sensor spatial scale; for example, a sensor averaging over scales of 100 m gains little from measurements faster than 0.1 Hz (once every 10 s), while a 1-m sensor will lose equivalent space resolution if averaging is done over periods exceeding 0.1 s.

On the basis of the arguments presented above, the ideal sensor for studying precipitation variability at small scales will be of the smallest size possible (matched with the appropriate averaging time) for which the field approximation of precipitation holds. Table 1 shows the number of raindrops hitting sensors of various sizes during a time corresponding to the sensor's natural averaging period for a typical stratiform rain rate (1 mm hr^{-1}). Table 1 shows that sensors much smaller than 1 m^2 are too small to sample the precipitation field properly, while sensors much larger than a square meter sacrifice resolution. Hence the ideal sensor must have a size of the order of a square meter with precipitation being averaged over periods of about 0.1 s. Additionally, the measurements must be achieved with as little quantization effects as possible caused by the sensor itself because the precipitation field statistics must remain uncontaminated by artificial sensor characteristics.

The "Sonic" Gauge Approach

Description of the Instrument

A simple way to study the precipitation fine structure over small space scales and timescales is to use an acoustic approach. Anyone who has been in a tent, trailer, or barn during rain will have noticed that the character and fine structure of rainfall can be identified by listening to the sound of raindrop impacts. It is this characteristic that is exploited in the development of a "sonic" gauge.

Figure 1 illustrates the principle of the sonic gauge. Hydrometeors fall on a "capture surface" (≈1 m^2) and the impacts produce sound or vibrations on the capture surface. The capture surface must transmit sound well even for tiny impacts like those produced by snowflakes but must not resonate excessively as resonance introduces additional time smoothing because of the decay time of the sound wave. The vibrations traveling through the middle point of the surface are reproduced on electric signal by a contact microphone attached below the surface. The vibration of the contact microphone produces an electric signal which is sent to a PC and digitized. A 0.1-s record of this signal proportional to the sound amplitude caused by impacts of ice pellets is also shown in Figure 1. As can be seen on Figure 1, the decay time of sound from each impact (less than 0.005 s) is much shorter than the natural averaging time (0.1 s) of a sensor of this size.

For each impact, the amplitude A of the vibration of the capture surface is proportional to the momentum mv of the hydrometeor at the time of impact. Over a given time period, one can compute the average momentum transfer per unit time $d(mv)/dt$ from hydrometeors striking the surface. However, the precipitation rate R is defined as the mass m (although expressed in height units) of water fallen per unit time (dm/dt). In calm winds, the three-dimensional velocity of hydrometeors v is approximately equal to their fall speed v_f. For raindrops, the fall speed of the drops is roughly proportional

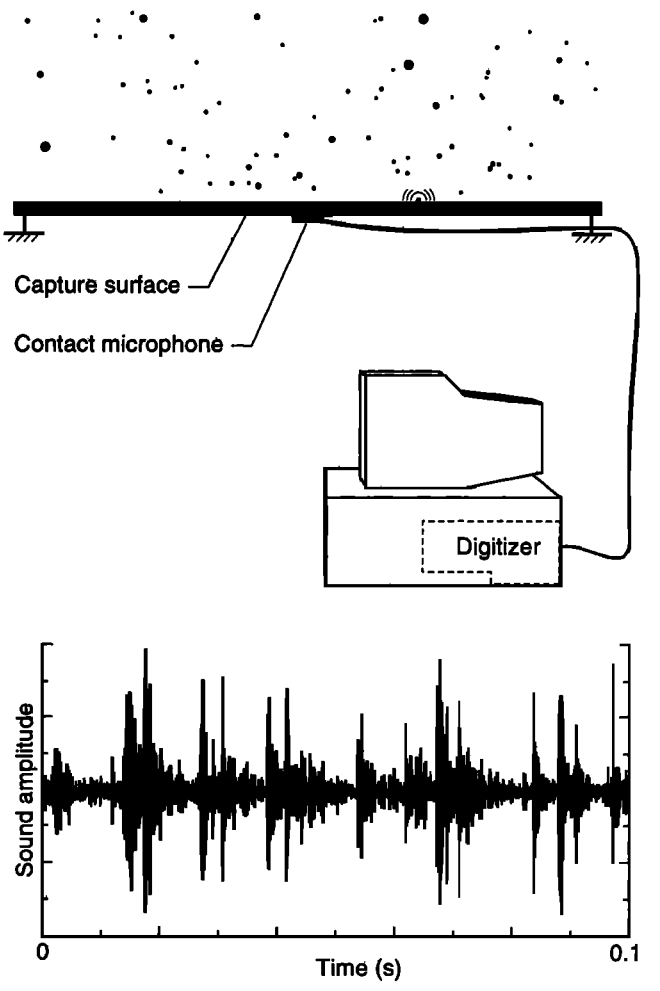

Figure 1. Schematic illustration of the sonic gauge. Hydrometeors fall on the capture surface, and the vibrations from their impacts travel in the surface to a contact microphone which converts the vibration of the surface into an electric signal digitized by a nearby PC. An example of such a recording is shown at the bottom of Figure 1.

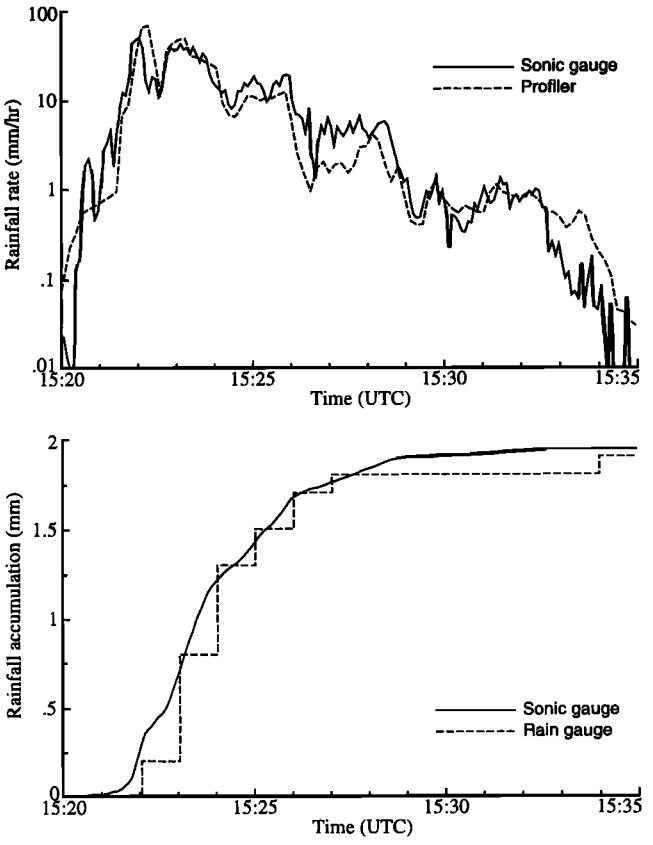

Figure 2. Comparisons of rainfall measurements made by the sonic gauge and other instruments during a Florida shower on August 1, 1995. (top) Rainfall rates derived from the sonic gauge data and wind profiler (radar) data taken at 300 m height. (bottom) Rainfall accumulations measured by the sonic gauge and a tipping bucket rain gauge.

to the square root of drop diameters [*Rogers and Yau*, 1989], or to $m^{1/6}$, so the sound amplitude A is roughly proportional to $R^{7/6}$. In snow, $v_f \propto d^{0.3}$ [*Langleben*, 1954], so $A \propto R^{3.3}$. The situation is more complex in the presence of winds close to the sensor level. Furthermore, even if the contribution from an average wind could be removed, the variability in that wind with time will introduce an artificial variability in A and hence R. To avoid this variability, the sonic gauge data were collected only when the surface horizontal wind was less than half the average fall speed of hydrometeors.

Data from the sonic gauge are processed as follows. The signal from the contact microphone is digitized by a commercial sound board for PCs at CD-like resolution (16-bit digitization at 44.1 kHz). Recordings are made over several 10-min periods in rain, ice pellets (sleet), and snow. The 10-min period is chosen because it is the longest period over which recordings can be made while sensor degradation caused by accumulation of water or snow on the capture surface is negligible. Vibrations of the contact microphone caused by hydrometeor impacts were found to have a natural frequency near 8.6 kHz. The data are therefore filtered to keep fluctuations around 8.6 kHz and eliminate other frequencies caused by neighboring sounds sources or 60-Hz contamination of the microphone signal. The envelope of the filtered signal is then retrieved, providing a measurement of the sound amplitude A as a function of time. This amplitude is then converted to a precipitation rate R based on the nature of hydrometeors. Collocated measurements of rainfall made by the sonic gauge, a rain gauge, and a radar wind profiler (Figure 2) suggest that the sonic gauge can measure rainfall with good accuracy over a large dynamic range of precipitation rates.

First Results

On December 28, 1994, in Montreal, Canada, a series of precipitation bands passed over the region associated with the approach of a cold front. The surface temperature was just over 0°C, and depending on the temperature profile in the first kilometer, which varied considerably over time, precipitation either fell as snow, ice pellets, or rain (with the snow melting at about 800 m). Eleven 10-min sound recordings were made on that day, five in rain and three each in ice pellets and snow.

To look at the character of precipitation variability as a function of scale, a power spectrum of retrieved precipitation intensity was constructed and is shown in Figure 3. Since the sonic gauge has a natural averaging scale of 1 m, any data for frequencies higher than about 10 Hz are affected by sensor averaging and are indicated by a dashed line in Figure 3. After a nonzero slope at low frequencies (compatible with scaling behavior), the power spectra show a clear change in slope at scales varying from 2 s (0.5 Hz or about 20 m) in rain to 20 s (0.05 Hz or 200 m) in snow. For ice pellets, which are formed by the partial melting of snow and its refreezing into a compact ice spheroid, the spectrum appears to show a combination of the power spectra in rain and snow. It should be noted that this behavior is much different than that expected from a reasoning like *Tessier et al.*'s [1993], where the power spectrum of precipitation intensity should follow a powerlaw down to the sensor resolution.

The sonic gauge data shows the existence of a clear break in the

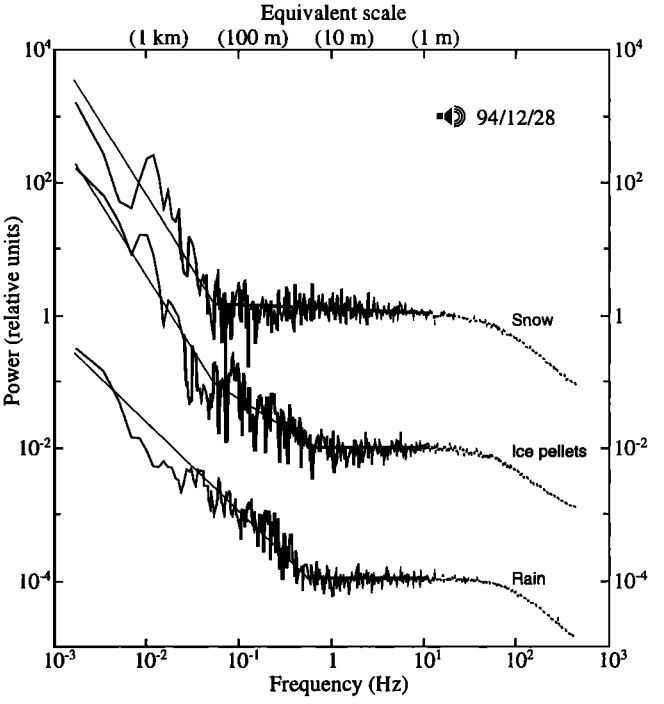

Figure 3. Normalized power spectra of precipitation rates as derived by the sonic gauge on December 28, 1994 in snow, ice pellets, and rain. The dashed lines above 10 Hz indicate timescales corresponding to spatial scales smaller than the sensor size. The equivalent scale was computed based on the 12.5 m-s^{-1} speed of weather echoes observed on that day. Spectra have been shifted for display.

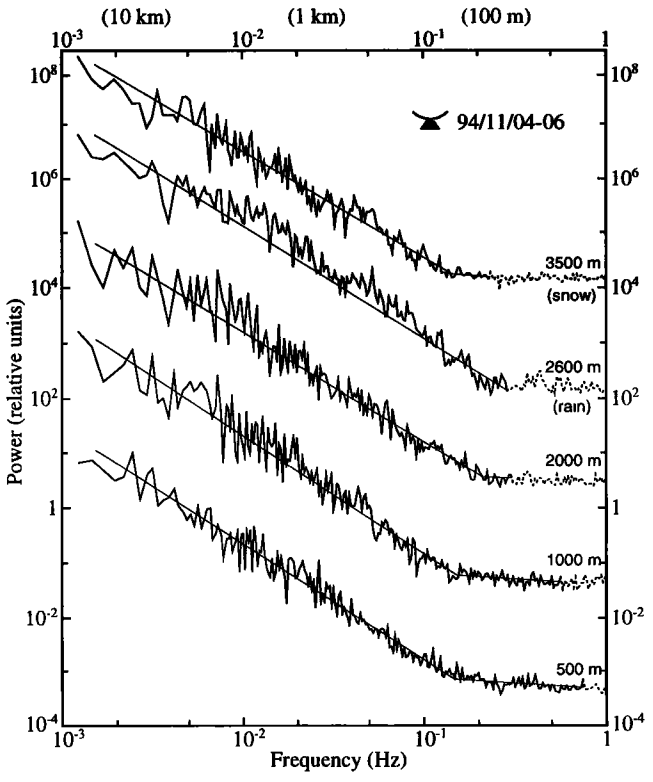

Figure 4. Normalized power spectra of precipitation rates as derived by the McGill vertically pointing radar between November 4 and November 6, 1994 at five different heights (500 m, 1000 m, 2000 m, and 2600 m in rain, and 3500 m in snow) over Montreal. On the basis of the wind speed measurements and an average fall speed of hydrometeors, the time of replacement of hydrometeors inside the volume sampled by the radar was computed, and timescales shorter than this replacement time are indicated by dashed lines. The equivalent scale was computed based on the 25-m s^{-1} speed of weather echoes.

power spectra for scales of several tens of meters. This occurs at a scale much larger than could be accounted for by sensor size. Furthermore, the fact that the scale at which this break appears varies significantly with precipitation type reinforces the likelihood that this observed change in the spatial structure of the precipitation field is not an artifact of the instrument. The reason for a break and a near white-noise variability at shorter scales is unclear using data from the sonic gauge alone. However, this break occurs at a scale large enough to be observed by other instruments such as narrow-beam radars collecting data at high space-time resolution.

Radar Data Revisited

On the basis of the insight gained using sonic gauge data, high resolution radar data in precipitation were then reexamined. Data were collected by the McGill X-band high-resolution vertically pointing radar [*Fabry et al.*, 1992] from November 4 to November 6, 1994. The radar measures the reflectivity of weather targets as they pass overhead with high temporal (0.5 s) and spatial (15 m) resolution. The pulse length used was 0.25 μs (giving a vertical averaging distance of 37.5 m), and the 2° beam width results in a cylindrical-shaped sampling volume whose diameter is 35 m at 1-km range.

Data from 11 hours of precipitation during this 3-day period were used. Time series of reflectivity at five heights, four in rain (500 m, 1000 m, 2000 m, and 2600 m) and one in snow (3500 m), were extracted and converted to precipitation rates. Power spectra of precipitation intensity for these five heights are shown in Figure 4. Here again, dashed lines indicate portions of the spectra affected by sensor averaging. The powerlaw behavior at low frequencies is observed to break for scales around 5 s (100 m), a scale much larger than the instrument's averaging scale at close range. More important is the fact that the location of the break occurs at lower frequencies (larger spatial scales) as we get closer to the ground, a behavior incompatible with an explanation of instrument smoothing. In this case too, the break between the strong powerlaw at low frequencies and the almost flat spectrum at high frequencies occurs at larger scales in snow just above the melting layer (3500 m) than in rain just below it (2600 m). This suggests that the melting layer reintroduces small-scale structure into the field.

This impression is reinforced by studying a portion of the data used in the analysis (Figure 5). This time-height section of reflectivity shows relatively little structure in snow just above the melting layer but considerably more variability just below the melting layer. This high variability gradually diminishes as rain falls toward the ground, a behavior compatible with a mixing process occurring

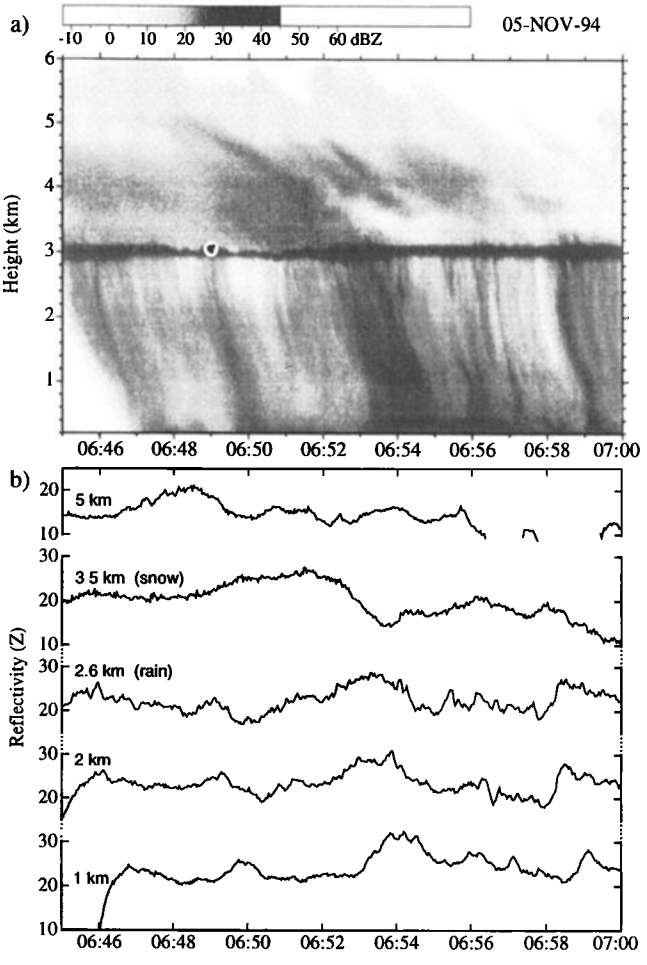

Figure 5. Portion of the radar data used in the analysis. (a) Time-height section of reflectivity collected by the vertically pointing radar between 0645 and 0700 UT on November 5, 1994 is shown. The region where melting occurs is clearly indicated by the bright band at 3 km. (b) Traces of reflectivity at five different heights during the same period, three in rain (1 km, 2 km, and 2.6 km) and two in snow (3.5 km and 5 km) are shown.

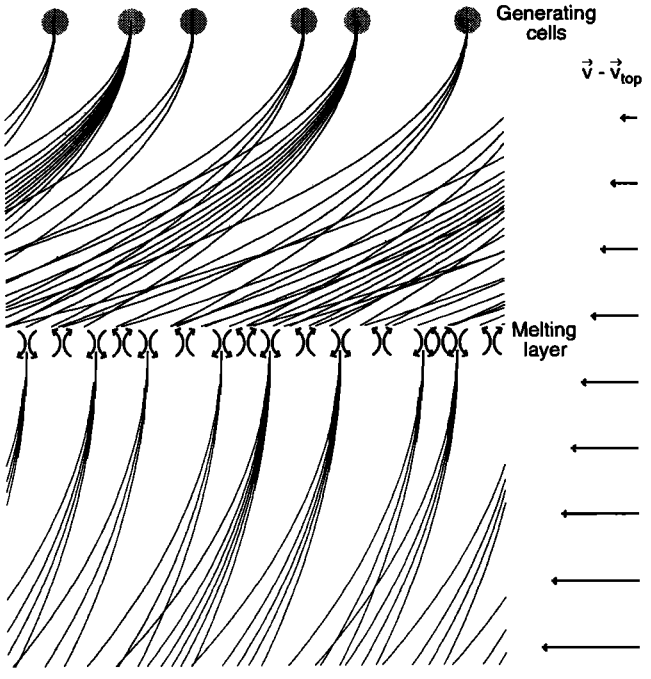

Figure 6. Calculated trajectories of hydrometeors produced by generating cells and subjected to a constant wind shear. Under such conditions, the differential fall speed of hydrometeors causes them to spread as they fall, and the precipitation field gradually loses its small-scale structure as a result. When snowflakes melt, the cellular circulation in the melting layer may regenerate some precipitation structure.

progressively with time. A similar but less striking behavior can be seen in the snow, where the greater variability can be seen at 5 km than at 3.5 km.

Interpretation

The data presented in the previous two sections suggest that this new regime in precipitation variability which appears for spatial scales of the order of 100 m is caused by a mixing-like process. It is unlikely that such mixing is caused by wind because the wind field shows scaling behavior down to millimeters. If the conditional sampling of sonic gauge data in nonwindy conditions may have caused a concern as to the reality of this break, the radar data, not subject to this constraint, clearly confirms the existence of the change in the regime of precipitation variability. As noted in the introduction, hydrometeors are not perfect passive tracers. The differential fall speeds between hydrometeors can provide an explanation for the appearance and gradual growth of this new regime.

Figure 6 presents the computed trajectories of hydrometeors originating at point sources and subjected to an hypothetical wind profile. Even if precipitation is generated from point sources, when submitted to a wind shear, hydrometeor trajectories will spread horizontally because of their different fall speeds. This spreading is a function of the magnitude of the wind shear and of the distribution of fall speeds and will result in an increasing loss of precipitation structure with distance below the generating cells.

This result can be approached more formally by quantifying how the trajectories spread from a point source continuously producing new hydrometeors. On a reference frame attached to that point source moving at a speed $\vec{v}_s$, the trajectory of hydrometeors is affected by their fall speed $v_f(h)$ and wind $\vec{v}(h)$, such that their horizontal position with respect to the point source $\vec{X}(h)$ can be found from [*Douglas et al.*, 1957]:

$$-\frac{d\vec{X}(h)}{dh} = \frac{\vec{v}(h)-\vec{v}_s}{v_f(h)}. \quad (1)$$

If one neglects changes in the vertical velocity of hydrometeors with height, the horizontal position of the hydrometeor at a height h is

$$\vec{X}(h) = \frac{1}{v_f}\int_h^{h_r} \vec{v}(z)-\vec{v}_s \, dz. \quad (2)$$

If the result of the integral is nonzero, which is generally the case, hydrometeors with different fall speed $v_f(h)$ will spread.

The additional structuring below the melting layer is more complex. A suggested explanation of the presence of stronger turbulence in the melting layer than above or below it was proposed by *Atlas et al.* [1969] and has been measured by *Willis and Heymsfield* [1989]. Melting-induced convection could be a mechanism responsible for the additional structure in the rain field. If a volume of air contains more melting snow than its surroundings, it will become cooler than its environment because of the removal of heat by melting. This cooler and denser parcel will tend to accelerate downward. Conversely, pockets containing less melting snow will accelerate upward. As a result, the precipitation flux is increased locally by the downward motion of regions with excess melting snow and is decreased by the upward motion of regions with less melting snow. Therefore, at the bottom of the melting layer, the number of raindrops per unit volume is increased below decaying downdrafts and decreased below forming updrafts, adding to the structure of the rain field below the melting layer compared to the snow field above.

While the spreading of raindrops explanation is based on nonturbulent concepts, it also applies in a turbulent environment. If the hydrometeors were perfect passive tracers and their trajectory only dictated by turbulence, then the scaling range observed for times larger than 10 s would likely extend to much smaller time scales and space scales. However, hydrometeors are not perfect tracers. First, they have inertia (and will resist organization at very small scales), but primarily they have fall velocities which are different for each of them. As a result, attempts by turbulence to organize them in clusters will be quickly defeated by the fact that drops of different sizes fall at different speeds and hence try to move apart. This effective spreading of hydrometeors therefore results in a phenomenon akin to mixing at small scales but occurring over scales of tens of meters instead of millimeters.

The effective mixing caused by the differential fall speed of hydrometeors will of course affect the power spectra of precipitation at small scales. The processes described above could explain why a regime with nearly whitenoise variability is present and progressively moves to larger scales as precipitation falls. The melting process recreates some of that lost structure (perhaps by the convection-related mechanism suggested), moving the low frequency powerlaw regime in precipitation back toward smaller scales. In the case of ice pellets (Figure 3), some weak melting circulation may have started to reorganize precipitation but not as significantly as in rain; as a result, the ice pellets spectrum shows some of the melting induced extension of the powerlaw regime, but it remains incomplete, as is the melting.

The low-frequency regime in precipitation variability observed in the sonic gauge and radar data seems to have its origin in the precipitation formation (Figure 4) and is likely closely linked with the turbulence basis proposed by *Lovejoy and Schertzer* [1986] and

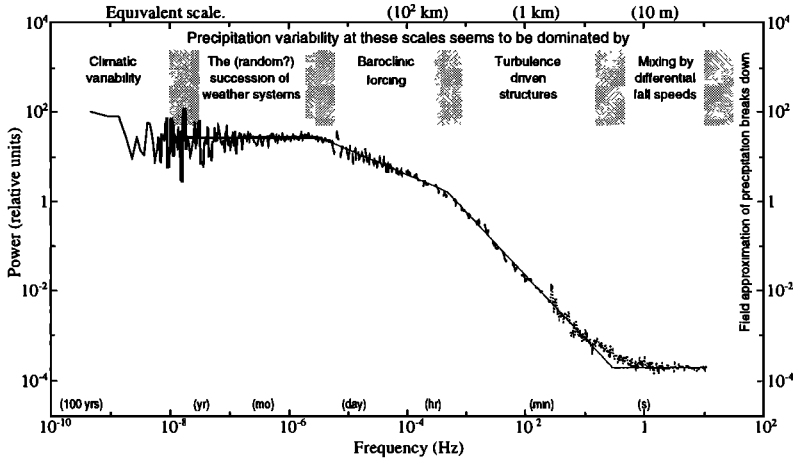

Figure 7. Normalized power spectrum of precipitation rates derived from three sources. The proposed interpretation of the various regimes are speculations. The data with the solid line are from daily observations of precipitation at McGill from 1924 to 1992; the data in dashed line are from 14 months of high resolution data from a drop-counting rain gauge taken between 1992 and 1994; sonic gauge data in rainfall over a month's period (August-September 1995) in Florida and Colorado were used for the dotted line. The power spectrum of sonic gauge data was artificially leveled with the two others to show the continuous "turbulence" regime observed regularly by radar data (Figure 4). Power law fits through the four regimes are also indicated: the slope in the "turbulence" regime is -1.40, while the slope in the "baroclinic" regime is -0.56. The equivalent scale was computed based on the 13.2-m s^{-1} average speed of weather echoes in Montreal computed by *Austin and Haynes* [1975].

Tessier et al. [1993]. This theory is strengthened by the fact that this regime is extended during the melting process by what appears to be convectively driven circulation, or enhanced turbulence, in the melting layer.

Using this new data, it may be interesting to reexamine the character of precipitation variability over a large range of scales. For this purpose, the data from daily precipitation at McGill since 1924, high-resolution rain gauge data taken in the past 3 years, and sonic gauge data were combined, and the result is plotted in Figure 7. Figure 7 suggests four or five regimes in variability. At high frequencies, the mixing by differential fall speeds dominates the variability up to about 50 to 100 m. The next regime which may be attributed to the structuring of precipitation by turbulence processes extends up to about 20 km. As the space scale increases (or frequency decreases), a new regime appears from about 50 km to 3000 km. It is interesting to note that such scales correspond to those associated with baroclinic forcing, from the width of frontal precipitation bands (of the order of 50 km) to the size of midlatitude cyclones (a few thousands of kilometers). While wind does not show such a clear break around 50 km [*Lilly and Petersen*, 1983], it is possible that the different instability in the atmosphere dominating precipitation formation at that scale (baroclinic vs. convective) may cause a different organization of the precipitation patterns and consequently a different regime in precipitation variability. Another possibility has been proposed by *Olsson et al.* [1993], who also observed a change in precipitation statistics at around 40 min and a week, in Sweden, and noted that these times corresponded to the average rainfall event duration and the average dry period, respectively. However, a plot of rainfall accumulation versus rainfall duration (Figure 8) suggest that while the average rainfall event is indeed around an hour, events longer than 40 min also have a different character than shorter ones, so this possibility may not completely explain our observations. A third possible explanation proposed by *Fraedrich and Larnder* [1993] is that the scaling break may be an artifact of the inability of the rainfall measuring instruments to measure frequent weak signals. Another scaling break occurs around 5 days because there is no larger precipitating system than those caused by baroclinic instability or because we have reached a timescale corresponding to the size of the Earth. Beyond that break, the spectrum is flat as the passage of weather systems with time over Montreal does not appear to show any nontrivial organization. This regime extends from a few days to a few years, beyond which precipitation variability is probably dominated by climate variability, although a lack of data in this range precludes us from seeing that signal well. Although the data in Figure 7 illustrate the presence of several regimes in the variability of precipitation with time, one can identify a region over 3

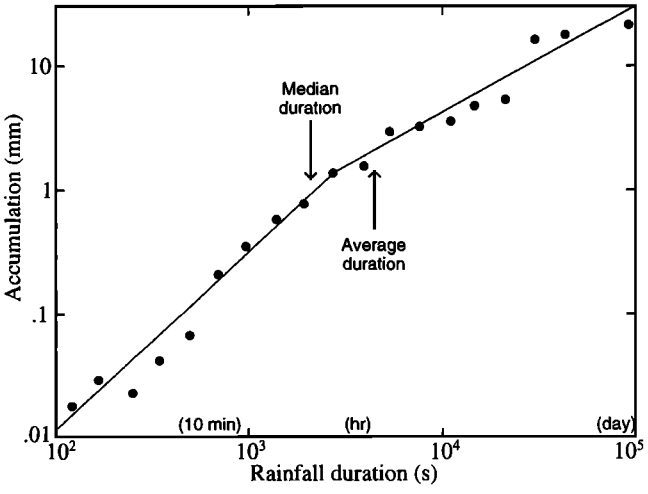

Figure 8. Average accumulation of rainstorms as a function of their duration. The 1101 rainfall events used in this graph (3 years of data from two gauges) were grouped in 20 categories of rainfall duration (spaced a factor of $2^{0.5}$ apart), and the average accumulation for each category is plotted. The median and average duration of rainfall events are also indicated.

orders of magnitude (a few seconds up to an hour) where the variability is compatible with scaling approaches. The regime may extend to larger scales if the break in the power law around an hour is instrument-related but will likely not extend below a few seconds because hydrometeors are not perfect passive tracers.

Conclusions

An effort has been made in this work to investigate the variability of precipitation particularly at small scales. To this end, data from a sonic gauge and a vertically pointing radar were used to study the precipitation fields at scales below 1 min in time or 1 km in space. These data show that precipitation variability at small scales (horizontal distances of less than a few tens of meters) has a much different character than at larger scales. This new regime appears to be the result of a mixing-like process caused by the differential fall speed of hydrometeors which tends to smear structures in the field.

This regime fixes a new lower limit to the scale up to which the turbulence-driven scaling regime extends. Nevertheless, scaling regimes compatible with a multifractal approach can still be observed over 3 orders of magnitude in time, from a few seconds to about an hour.

Appendix: From Time to Space Statistics in Rain

The data collected in this work are all time series of rainfall at the ground (gauges) or of reflectivity at a given height (radar). As a result, all statistics computed with these data are temporal in nature. While interesting per se, these statistics would bring more insights to the physics of the phenomenon observed if they could be converted into space statistics. When trying to convert time statistics to space statistics, at least three approaches are possible:

1. The space-time relation involves a scale-dependant turbulent velocity. For a turbulent atmosphere, what is significant for space-time conversion is not the absolute velocity but rather the differential velocity/shear across structures of a given size. If one uses the theoretically justified, empirically substantiated Kolmogorov velocity (see *Tessier et al.* [1993] for theory and practice in rain), then one obtains

$$\Delta t(\lambda\Delta x) = \lambda^{1-H}\Delta t(\Delta x),$$

where H is empirically found to be close to the Kolmogorov value of 1/3 and λ is the factor by which the space scale is changed.

2. The patterns of precipitation are sufficiently frozen (evolution is slow compared to advection) that Taylor's hypothesis may be used, resulting in a scale-independant conversion velocity between time and space statistics.

3. The dynamics of the rainfall process are so complex that trying to convert time statistics to space statistics is impossible or hopeless.

The choice of the method used is crucial, as it can radically change the conclusions that can be made from the measurements. For example, using the first method, if one uses 10 m s^{-1} as a typical velocity for synoptic scale motions (1000 km), then we find that the time scale associated with a 1 m space scale is $10^6/10*(10^{-6})^{(1-1/3)} = 10$ s, which corresponds to the break observed in the sonic gauge statistics. Using this approach, the 10-s break is then an artifact caused by the 1-m scale of the instrument, not a meteorologically significant observation. To make the best choice of the method to use, one must try to make predictions with each and see if they can be verified using data.

Let us suppose that the first method is correct. Then, for radar observations at 1 km altitude which have an inherent scale of 35 m (both from the pulse length and the beam width), an instrument-induced break should be observed at a timescale of $10^6/10*(35*10^{-6})^{(1-1/3)} = 107$ s. However, radar observations in this paper and elsewhere show a break at 10 s, well below what can be attributed to instrument scale. Hence the scale-dependant velocity method seems to be incompatible with the data. If we use a scale-independant approach, then the 10-s break observed in the gauge data is meteorologically significant and should also be observed by the radar at 10 s too, which turns out to be the case. On the basis of these arguments, a scale-independant velocity was chosen for converting time statistics to space statistics. Whether the result of this exercise simply reflects the fact that approaches used in turbulence theory may not apply directly to precipitation measured at the ground or implies something more profound is beyond the scope of this contribution.

Acknowledgments. I wish to thank Aldo Bellon and Isztar Zawadzki from the J.S. Marshall Radar Observatory of McGill University for providing the radar data used in this study as well as valuable advice, and Peter Hildebrand and Charles Frush from NCAR's Remote Sensing Facility for supporting and helping in the development of the sonic gauge. The National Center for Atmospheric Research is sponsored by the National Science Foundation.

References

Atlas, D., R Tatehira, R.-C. Srivastava, W. Marker, and R.E Carbone, Precipitation induced mesoscale wind perturbations in the melting layer, *Q. J. R. Meteorol. Soc., 95*, 544-560, 1969.

Austin, G.L , and M. Haynes, Comparative study of maritime tropical and temperate continental precipitation patterns, Paper presented at 16th Conference on Radar Meteorology, Am Meteorol Soc , Houston, Tex., 1975.

Austin, P M., and R A. Houze, Analysis of structure of precipitation patterns in New England, *J. Appl. Meteorol., 11*, 926-935, 1972

Douglas, R.H , K.L S. Gunn, and J S. Marshall, Pattern in the vertical of snow generation, *J. Meteorol., 14*, 95-114, 1957.

Duncan, M.R., F Fabry, S. Lovejoy, and D Schertzer, The multifractal radar Observer's Problem, Paper presented at 26th International Conference on Radar Meteorol., Am Meteorol Soc , Norman Okla., 1993.

Fabry, F , G.L. Austin, and D Tees, The accuracy of rainfall estimates by radar as a function of range, *Q. J. R. Meteorol. Soc., 118*, 435-453, 1992.

Fraedrich, K., and C. Larnder, Scaling regimes of composite rainfall time series, *Tellus Ser. A , 45*, 289-298, 1993.

Georgakakos, K.P., A.A. Carsteanu, P.L. Sturdevant, and J.A. Cramer, Observations and analysis of midwestern rain rates, *J. Appl. Meteorol., 33*, 1433-1444, 1994.

Gupta, V.K , and E.C Waymire, A statistical analysis of mesoscale rainfall as a random cascade, *J. Appl. Meteorol., 32*, 251-267, 1993

Kumar, P., and E. Foufoula-Georgiou, A multicomponent decomposition of spatial rainfall fields, 2, Self-similarity in fluctuations, *Water Resour. Res., 29*, 2533-2544, 1993.

Langleben, M.P , The terminal velocity of snowflakes, *Q. J. R. Meteorol Soc., 80*, 174-181, 1954.

Lilly, D.K., and E.L. Petersen, Aircraft measurements of atmospheric kinetic energy spectra, *Tellus, Ser. A, 35*, 379-382, 1983.

Lovejoy, S., and D. Schertzer, Scale invariance, symmetries, fractals, and stochastic simulations of atmospheric phenomena, *Bull. Am. Meteorol. Soc., 67*, 21-32, 1986.

Lovejoy, S., and D. Schertzer, Fractals, rain drops and resolution dependance of rain measurements, *J. Appl Meteorol., 29*, 1167-1170, 1990.

Marshall, J S., Precipitation trajectories and patterns, *J. Meteorol., 10*, 25-29, 1953.

Marshall, J.S , and W Hitschfeld, Interpretation of the fluctuating echo from randomly distributed scatterers, 1, *Can. J. Phys., 31*, 962-994, 1953

Olsson, J., J. Niemczynovicz, and R. Berndtsson, Fractal analysis of

high-resolution rainfall time series, *J. Geophys. Res.*, *98*, 23,265-23,274, 1993.

Over, T.M., and V.K. Gupta, Statistical analysis of mesoscale rainfall: Dependence of a random cascade generator on large-scale forcing, *J. Appl. Meteor.*, *33*, 1526-1542, 1994.

Rogers, R.R., and M.K. Yau, *A Short Course in Cloud Physics*, 3rd Ed., 293 pp., Pergamon, Tarrytown, N.Y., 1989.

Schertzer, D., and S. Lovejoy, Physical modeling and analysis of rain and clouds by anisotropic scaling multiplicative processes, *J. Geophys. Res.*, *92*, 9692-9714, 1987.

Tessier, Y., S. Lovejoy, and D. Schertzer, Universal multifractals: Theory and observations in rain and clouds, *J. Appl. Meteorol.*, *32*, 223-250, 1993.

Willis, P.T., and A.J. Heymsfield, Structure of the melting layer in mesoscale convective system stratiform precipitation, *J. Atmos. Sci.*, *46*, 2008-2025, 1989.

F. Fabry, National Center for Atmospheric Research, Advanced Study Program, P.O. Box 3000, Boulder, CO 80307-3000.

(Received March 23, 1995; revised February 6, 1996; accepted February 12, 1996.)